Random but Limited Pressure of Graphene Liquid Cells

Hirokawa, Sota
Department of Aeronautics and Astronautics, Kyushu University

Teshima, Hideaki
Department of Aeronautics and Astronautics, Kyushu University

Solís-Fernández, Pablo
Global Innovation Center, Kyushu University

Ago, Hiroki
Global Innovation Center, Kyushu University

他

https://hdl.handle.net/2324/6786359

出版情報：Ultramicroscopy. 250, pp.113747-, 2023-04-25. Elsevier
バージョン：
権利関係：

Random but Limited Pressure of Graphene Liquid Cells

Sota Hirokawa,[1,2] Hideaki Teshima,[1,2] Pablo Solís-Fernández ,[3] Hiroki Ago,[3] Qin-Yi Li,[1,2] and Koji Takahashi[1,2*]

[1] Department of Aeronautics and Astronautics, Kyushu University, 744 Motooka, Nishi-ku, Fukuoka 819-0395, Japan

[2] International Institute for Carbon-Neutral Energy Research (WPI-I2CNER), Kyushu University, 744 Motooka, Nishi-ku, Fukuoka 819-0395, Japan

[3] Global Innovation Center, Kyushu University, 6-1 Kasuga-koen, Kasuga, Fukuoka 816-8580, Japan

*Email: takahashi@aero.kyushu-u.ac.jp

ABSTRACT

Even though many researchers have used graphene liquid cells for atomic-resolution observation of liquid samples in the last decade, no one has yet simultaneously measured their three-dimensional shape and pressure. In this study, we have done so with an atomic force microscope, for cells with base radii of 20–134 nm and height of 3.9-21.2 nm. Their inner pressure ranged from 1.0–63 MPa but the maximum value decreased as the base radius increased. We discuss the mechanism that results in this inverse relationship by introducing an adhesive force between the graphene membranes. Also, the sample preparation procedure used in this experiment is highly reproducible and transferable to a wide variety of substrates.

KEYWORDS

Graphene liquid cells; Transmission electron microscopy; Atomic force microscopy; Pressure; Three-dimensional shape

1. Introduction

Transmission electron microscopy (TEM) observations by using graphene liquid cells (GLCs), which encapsulate the liquid between two graphene membranes, allow for visualization of phenomena in liquids with sub-second time resolution and atomic-level spatial resolution[1–4]. GLCs have been used in many research areas—such as crystallization[5–8], biological samples[9–12], lithiation[13,14], and the unique behavior of nanoscale bubbles[15–19]. First-generation GLCs (termed veil-type[3], which simply sandwich a liquid sample between two sheets of graphene) are used by many researchers today. The ease of preparation—requiring only graphene, a TEM grid and a liquid sample—has contributed substantially to the popularity of veil-type GLCs.

To date, several preparation methods for veil-type GLCs have been proposed[20–23]. The direct method, in which a sample droplet is sandwiched between two graphene-transferred TEM grids, is most commonly used[24]. However, veil-type GLCs have some disadvantages: the shape is not controllable because it depends on how a droplet randomly collapses into many tiny cells during the adhesion of two graphene sheets, and the number density of GLCs depends on the fabricator's skill. In particular, the height (thickness) of veil-type GLCs has rarely been discussed in the literature, even though the height effects on particle motion and crystal growth mode have been recognized[25,26]. Some studies have reported the height of GLCs by the log-ratio method[27–29] or direct measurement by atomic force microscopy (AFM)[5]. However, such studies have reported the height of only one or a few GLCs, and the relationship with the area and planar shape of each GLC obtained by TEM images has not been clarified. Furthermore, although liquid samples enclosed in a nanoscale space are considered to be under high pressure, there is only one report of an actual measurement of GLC pressure (by Ghodsi et al.[30]). They estimated the pressure of three GLCs by applying the density of water molecules (determined from the electron energy loss spectroscopy plasmon peak of water) to the equation of state of bulk water, and reported a high value ranging 100–400 MPa. Because the pressure of GLCs influences the crystal growth[25] and thermal behavior of the liquid, pressure information is necessary for an accurate discussion. To complete the missing information, we report the results of simultaneous AFM measurements of the three-dimensional (3D) geometry and internal pressure of GLCs.

2. Experiment

Fig. 1 shows the sequence of our sample fabrication. Each stacked layer is described from the top (e.g., top-middle-bottom). The first step was cutting 6 mm × 6 mm monolayer graphene on a Cu thin film and spin-coating polymethyl methacrylate (PMMA) onto the graphene [Fig. 1(a)]. The sample was baked on a hot plate at 80°C for 10 min. Cu was then etched by floating PMMA-graphene-Cu in a 0.2-M ammonium persulfate (APS) solution for 4 h [Fig. 1(b)]. PMMA-graphene floating in APS was gently scooped up with a glass slide and repeatedly rinsed through floatation in a sequence of solutions: a 4% (v/v) aqueous HCl solution followed by deionized water. The rinsed PMMA–graphene was moved to a Petri dish filled with pure water and scooped up with another graphene-Cu [Fig. 1(c)]. This process resulted in the encapsulation of water and the formation of hemispherical GLCs. Using as-grown graphene to scoop up the floating PMMA-graphene ensures a clean interface between both graphene layers. The PMMA-GLC-Cu was heated on a hot plate at 40°C for 10 min to help adhere the top and bottom graphene [Fig.1(d)], and then dried thoroughly. Next, PMMA-GLC-Cu was floated in a new

APS solution to etch the Cu film [Fig. 1(e)]. After rinsing as described, PMMA-GLC was floated in pure water and scooped up with the target substrate [Fig. 1(f)]. After scooping up the PMMA-GLC, the water on the back side of the substrate was removed with filter paper, and the substrate was heated on a hot plate at 150°C for 10 min to strengthen the bond between the substrate and graphene [Fig. 1(g)]. After the sample was dried sufficiently, it was submerged into a beaker of acetone at 50°C for 3–5 h to remove the PMMA [Fig. 1(h)]. The layer number and quality of the graphene were confirmed by Raman spectrum[31] and seleceted area electron diffraction (Fig. S1 in supplementary information). In this study, GLCs were transferred onto a 10 mm × 10 mm Si substrate for AFM measurements and onto a 3-mm diameter TEM grid. We do not recommend cutting graphene smaller than 6 mm square. If the graphene is cut too small, it will be easily bent during the Cu etching and will also peel off from the grid during the PMMA etching. Generally, preparation of GLCs with monolayer graphene is difficult because the graphene is brittle and tears off during transfer. However, in our attempts, our method has not failed in more than 10 attempts, and the number density of liquid pockets was higher than that fabricated by the aforementioned direct method.

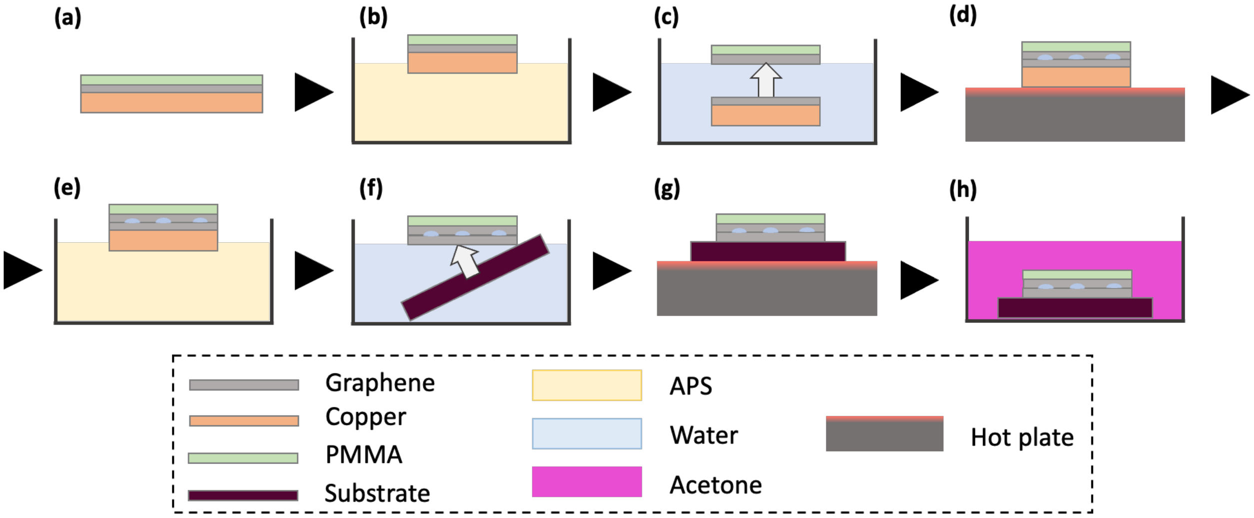

Fig. 1 Schematic of sample fabrication. The fabrication process involves spincoating PMMA on monolayer graphene (a), etching the Cu film (b), encapsulating water to form GLCs (c-d), and transferring the PMMA-GLC to the target substrate (e-g). The PMMA is then removed to complete the sample preparation (h).

We measured the three-dimensional geometrical data of GLCs on a Si substrate by AFM (SPM-8100FM, Shimadzu Corporation, Japan). The height was directly obtained using the built-in AFM software, and the area and perimeter of GLCs were manually measured using ImageJ[32]. We also recorded the deflection and piezo position of the AFM probe as it approached and was pushed into the GLCs. To convert the relationship between the deflection (recorded as a voltage) into force, we calculated the sensitivity [m/V] and spring constant [N/m] of the AFM probe using thermal tune method [33].

3. Results & Discussion

We observed a sample on a TEM grid using TEM, JEM2100plus (JEOL, Japan), at an acceleration voltage of 200 kV. We visualized water trapped between graphene; this water had a darker contrast than graphene [Fig. 2(a)]. GLCs were ca. 50–300 nm in size and circular, triangular, or square. More than half of the GLCs were connected to each other by wrinkle-like structures with a width of a few nanometers. In this paper, GLCs that were isolated from other cells are termed isolated cells and GLCs connected to other cells are termed connected cells. There was PMMA residue on the sample surface; this contamination may interfere with observation as it exhibits similar contrast to GLCs in TEM images. PMMA contamination can be easily distinguished from GLCs by their distinct shape differences. For instance, PMMA contamination typically exhibits a rectangular shape with dimensions of tens to hundreds of nanometers in width and hundreds to thousands of nanometers in length. Meanwhile, GLCs may exhibit a smaller and polygonal shape. Furthermore, GLCs can be readily differentiated by observing the nucleation of bubbles, as electron beams cause water to decompose and produce hydrogen gas[34,35].

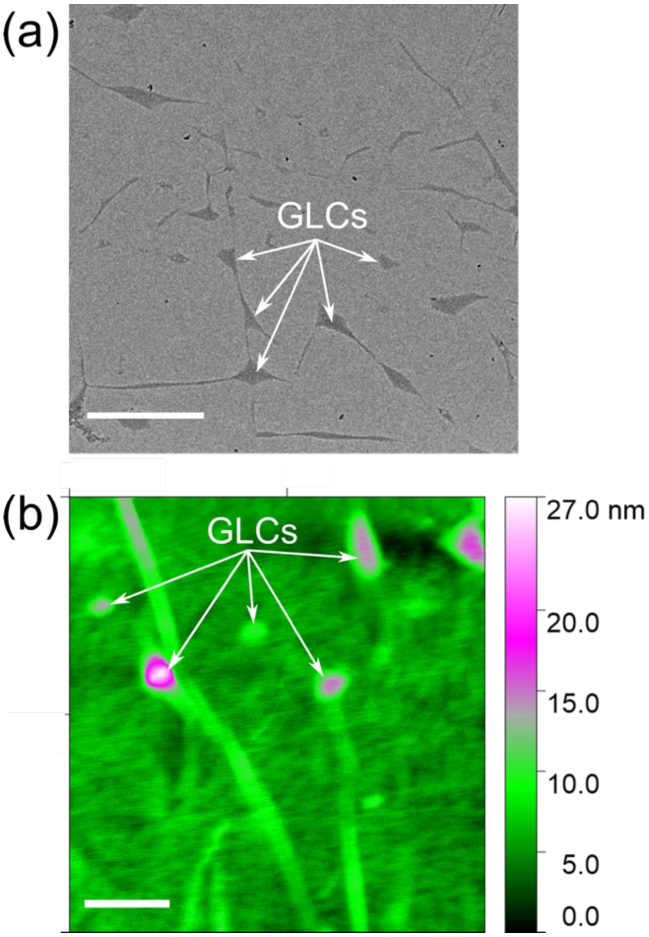

Fig. 2 (a) TEM image of GLCs on a TEM grid showing light gray graphene with scattered dark gray confined water. Scale bar is 500 nm. (b) AFM image of GLCs on a Si substrate with the color bar indicating height. Scale bar is 200 nm.

We then measured 53 GLCs on a Si substrate by AFM. Fig. 2(b) shows one of the AFM height images. We fabricated similar GLCs on a TEM grid and a Si substrate, and distinguished connected cells from isolated cells. The minimum and maximum areas of GLCs were 1306 and 56,019 nm^2, respectively. As a more intuitive value, here we define the equivalent radius as $r_{eq} = \sqrt{Area/\pi}$; minimum radius is 21 nm and maximum radius is 134 nm. The minimum and maximum heights of the GLCs were 3.9 and 21.2 nm, respectively. Fig. 3(a,b) shows plots of the height versus r_{eq} of isolated and connected cells. These GLCs had different height/radius correlation. Connected cells exhibited a clear trend of increasing height with increasing r_{eq}, with height/radius ratios in the range of 0.09–0.14 [Fig. 3(a)]. However, there was no clear trend between the radius and height in isolated cells [Fig. 3(b)]. Although the mechanism underlying these trends is an intriguing subject for further investigation, it falls outside the scope of this paper. In addition, we used $circularity = 4\pi \times area/perimeter^2$ (1.0 for a circle) as a representative value for the basal shape and investigated its relationship with the radius as well as height. Isolated cells seemed to have a more circular shape than connected cells; but there was no clear correlation between the circularity, base area, and height.

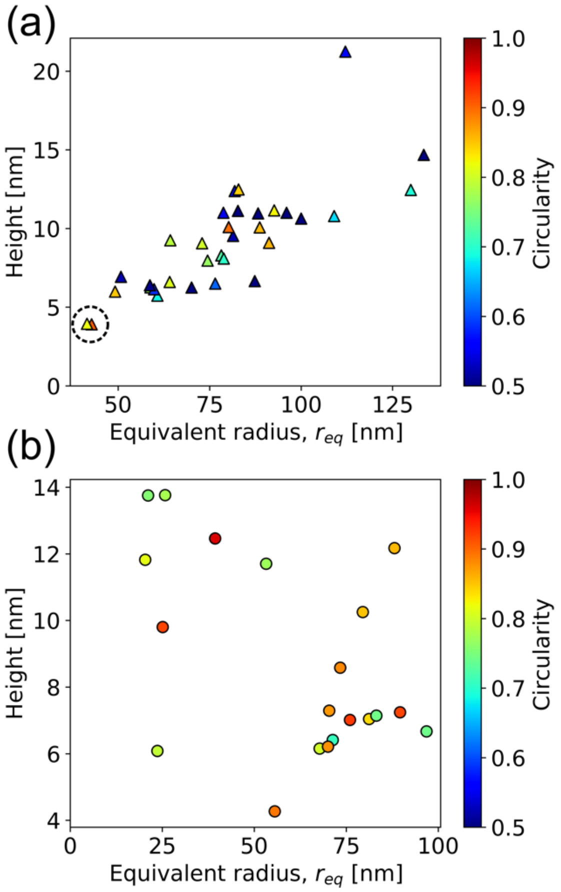

Fig. 3 Graph of GLC height versus corresponding equivalent radius obtained by AFM. (a) Connected cells and (b) isolated cells. The color of each marker represents the circularity of each GLC, reflecting the basal shape of the GLCs. The two GLCs encircled by the dashed line in (a) had similar geometry but varying pressure (48 MPa for smaller and 4 MPa for bigger GLC).

Subsequently, we calculated the pressure for each of the 53 GLCs in which we measured 3D shapes. First, we obtained a force–displacement curve (FDC) for each cell, which shows the relationship between the force applied to the AFM probe and the displacement between the tip of the AFM probe and the sample surface. The internal pressure was calculated based on the linear relationship between the indentation force and displacement of pressurized elastic shells as reported by Vella et al[36]. The calculation was performed using Eq. (1):

$$p_{vella} = \frac{F}{\pi R \delta} + p_0 \tag{1}$$

where F [N] is the indentation force, δ [m] is the indentation depth, R is the radius of curvature calculated from the equivalent radius and height of the GLC, h, $R = h/2 + r_{eq}^2/2h$, p_0 [Pa] is atmospheric pressure and p_{vella} [Pa] is the internal pressure (absolute pressure). It is important to note that Eq. 1 is valid only if the deformation is much larger than the thickness of the film, and therefore it can be applied in this experiment only if the indentation depth δ is much greater than the thickness of the single layer graphene (0.335 nm). To obtain a reliable result, we extracted the slope of the FDC when the indentation depth was more than 0.9 nm. The calculation procedures of force-indentation depth ratio is explained in the supplementary information.

However, because Eq. (1) does not take into account the stiffness of the graphene membrane, p_{Vella} overestimates the inner pressure of GLCs. As graphene is extremely stiff[37], it is necessary to consider the force of the graphene membrane to push back against the AFM probe, F_{graphene} [N]. Since the AFM probe tip radius, a, was approximately 7 nm, which is sufficiently smaller than the diameter of the GLC, we could calculate $F_{graphene}$ as the force required to indent graphene suspended on a circular hole to a depth δ using Eq. (2)

$$F_{graphene} = \frac{2\pi\sigma\delta}{\ln\frac{r_s}{a}} + \frac{E(q\delta)^3}{r_s^2}, \tag{2}$$

where σ and E are the two-dimensional (2D) pretension and 2D effective Young's modulus of single-layer graphene, respectively, with values of σ = 0.085 nN/m and E = 340 N/m obtained from previous studies[38,39]. Parameter r_s is the radius of suspended graphene, which was set to the equivalent radius. The parameter q is the coefficient obtained from Poisson's ratio, which is ca. 1.02 for monolayer graphene[38]. By dividing $F_{graphene}$ by the contact area between the probe and graphene, we can obtain the overestimated pressure. The contact area between AFM probe and graphene can be calculated as $A_{contact} = 2\pi a\delta$ by assuming that the probe tip is a sphere. Finally, Eq. (3) shows the true GLC internal pressure p.

$$p = p_{vella} - \frac{F_{graphene}}{A_{contact}} \tag{3}$$

The overestimation of p_{vella} reached more than 2% for all of GLCs and 10% for 26 out of 53 GLCs. Additionally, 6 GLCs showed a pressure overestimation more than 40%. These results suggest that factoring in the stiffness of graphene is essential when calculating the pressure of GLCs.

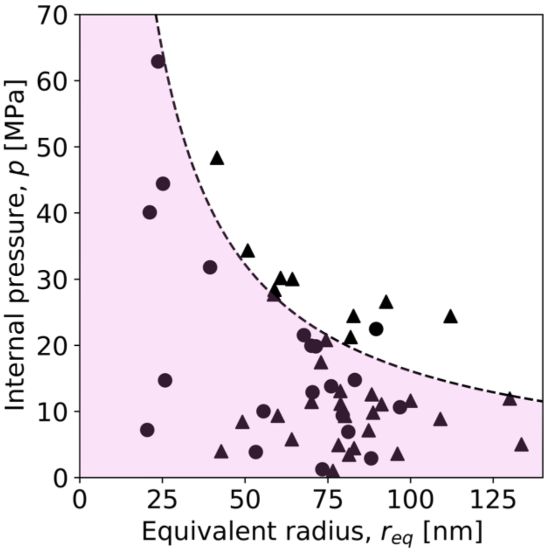

Fig. 4 Pressure distribution of GLCs. Triangular and circular markers represent connected and isolated GLCs, respectively. The colored area underneath the curve indicates the value lower than the upper estimate of the inner pressure when adhesive force between upper and lower graphene is 0.81 N/m.

We plotted p against *the* r_{eq} of each GLC in Fig. 4. The minimum pressure was 1.0 MPa (9.87 atm) and the maximum pressure was 63 MPa (622 atm), confirming that the water that was scooped up and confined in the graphene was several tens to several hundred times higher than atmospheric pressure. Fig. 4 indicates that a smaller radius corresponds to a higher maximum pressure. However, the relationship between the height and pressure is not as clear as that between the radius and pressure (refer to the supplementary information, Fig. S6). Furthermore, there was no difference in the pressure–radius relationship between isolated and connected cells. In the theoretical calculation presented by Ghodsi et al., the pressure of a GLC is unequivocally defined by the radius, height, and radius/height ratio; the internal pressure decreases as the height and radius increase[30]. However, our experiments confirmed that experimental GLCs differ from theory and exhibit different pressures, even for similar shapes. For example, the pressures of the two GLCs encircled by the dashed line in Fig. 3(a) that have similar geometries, were 48 MPa and 4 MPa, respectively.

There was a trend between the radius and maximum pressure at each radius. We hypothesize that this relationship between p and r_{eq} can be explained by considering how the GLCs reaches steady-state form. When the PMMA-graphene is scooped by graphene-Cu and top and bottom graphene sandwich the initial large droplet (Fig. 1(c)), the graphene layers bind to each other with a unit-length adhesive force γ [N/m] acting at the perimeter of the cell, $2\pi r_{eq}$ [m]. However, the encapsulated droplet starts to push the graphene, with an internal pressure p corresponding to its size. The force of the internal pressure p to peel the graphene is calculated as $p\pi r_{eq}^2$ [N]. The GLC shrinks to a shape in which these two forces are balanced, $2\pi r_{eq}\gamma = p\pi r_{eq}^2$, such that the relationship between the internal pressure and the radius is inversely proportional, $p = 2\gamma/r_{eq}$. The dashed line in Fig. 4 shows the inversely proportional fitting curve for maximum pressure and radius, $p = 1.62/r_{eq}$, from which the adhesive force γ was 0.81 N/m. The theoretical value of adhesive force between graphite layers is 0.29 N/m[40], so our estimation value is in the same order. If the adhesive force acting on all GLCs is equal to the attractive force between graphene, then the GLC pressures align at the maximum pressure. However, this is not the case in practice (Fig. 4). We presume that the contamination prevents ideal adhesion[41]; thus, there are GLCs with various low pressures.

To what extent does the presence of contamination impact the adhesion force between graphene layers? The adhesive force is primarily governed by the van der Waals energy[40]. Thus, we considered the van der Waals energy for a system with contamination between the two graphene layers. The van der Waals energy per unit area, $\prod$ [N/m], is given by the following Eq. (4)[42], with negative values indicating attraction:

$$\Pi = -\frac{A}{12\pi D^2} \tag{4}$$

where D [m] is the distance between the graphene layers, i.e., the thickness of the contamination; A [J] is the Hamaker coefficient, which is calculated using Eq. (5)[42]:

$$A = \frac{3}{4} k_B T \left(\frac{\epsilon_{Gr} - \epsilon_C}{\epsilon_{Gr} + \epsilon_C} \right)^2 + \frac{3h\nu_e}{16\sqrt{2}} \frac{(n_{Gr}^2 - n_C^2)^2}{(n_{Gr}^2 + n_C^2)^{3/2}} \tag{5}$$

where k_B [J/K] is the Boltzmann constant, T [K] is the temperature, h [J s] is the Planck constant, ε [-] is the dielectric constant, n [-] is the refractive index, ν_e [s^{-1}] is the main electronic absorption frequency (typically around 3×10^{15} s^{-1}) and the subscripts “Gr” and “C” refer to graphene and contamination, respectively. The values for graphene are ε_{GR} = 6.9[43], n_{Gr} = 2.6988[44], and for contamination are ε_C = 2.25 and n_C = 1.5[42], assuming that the contamination is hydrocarbons.

Considering a distance of D = 0.67 nm between the graphene layers as a case with a small amount of contamination adhesion, Eq. (4) shows that the adhesion force between the graphene layers is 0.013 N/m, which is dramatically reduced to approximately 1.6% of the maximum adhesion force of 0.81 N/m. The net reduction of the adhesion force should be dependent on the ratio of the surface area between clean and contaminated graphene. In conclusion, contamination significantly reduces adhesion, and its random distribution results in a random pressure for GLCs with the same radius. To prevent randomness of the internal pressure of GLCs, it is necessary to clean the graphene surface. Various cleaning methods have been proposed, such as electrostatic force cleaning with fine cloth fibers, air-assisted plasma, and annealing[45]. However, cleaned graphene surfaces can become contaminated soon after cleaning[46], so it is crucial to perform cleaning immediately prior to fabrication.

4. Conclusion

In this research, we contributed to the understanding of GLCs by performing the first simultaneous measurement of 3D shape and inner pressure using AFM. Our results showed that when GLCs were connected to each other with a cord-like structure, the bottom area and height increased proportionally, while this trend was not observed in isolated GLCs. We also pressed the GLC's apex using an AFM probe and measured the force-displacement curve. From the force-displacement curve, we calculated the inner pressure of GLCs and investigated the relationship between the pressure and basal area, the height, and the presence or absence of cell-to-cell connections. We confirmed that the pressure inside the GLCs reaches several hundred times greater than atmospheric pressure. Furthermore, we found that GLC's pressure is not solely determined by its geometry but rather is influenced by the surface contamination that decreases the adhesion force between top and bottom graphene. Our findings provide new insight. The 3D shape and pressure data provided in this paper will serve as a critical reference to understand the phenomena inside GLCs.

Conflict of Interest

The authors have no conflicts to disclose.

Acknowledgment

This work was partially supported by the Japan Science and Technology Core Research for Evolutional Science and Technology (CREST) (grant no. JPMJCR18I1), the Japan Society for the Promotion of Science Grants-in-Aid for Scientific Research (KAKENHI) (grant nos. JP20H02089 and JP21K18693, JP21K20405), and Grant-in-Aid for JSPS Fellows (grant no. JP21J21976). We thank Tatsuya Ikuta and Kazuhiko Morishita for fruitful discussions and technical support. Also, I am grateful to Hori Kawamoto for his assistance with the initial experiments.

Data Availability

The data that support the findings of this study are available from the corresponding author upon reasonable request.

References

[1] J. M. Yuk, J. Park, P. Ercius, K. Kim, D. J. Hellebusch, M. F. Crommie, J. Y. Lee, A. Zettl, and A. P. Alivisatos, Science **336**, 61 (2012).

[2] N. Clark, D. J. Kelly, M. Zhou, Y.-C. Zou, C. W. Myung, D. G. Hopkinson, C. Schran, A. Michaelides, R. Gorbachev, and S. J. Haigh, Nature (2022).

[3] J. Park, K. Koo, N. Noh, J. H. Chang, J. Y. Cheong, K. S. Dae, J. S. Park, S. Ji, I.-D. Kim, and J. M. Yuk, ACS Nano **15**, 288 (2021).

[4] X. Gao, L. Zheng, Y. Yao, and H. Peng, Adv. Funct. Mater. 2202502 (2022).

[5] M. Jeong, J. M. Yuk, and J. Y. Lee, Chem. Mater. **27**, 3200 (2015).

[6] L. Chen, A. Leonardi, J. Chen, M. Cao, N. Li, D. Su, Q. Zhang, M. Engel, and X. Ye, Nat. Commun. **11**, 3041 (2020).

[7] K. S. Dae, J. H. Chang, K. Koo, J. Park, J. S. Kim, and J. M. Yuk, ACS Omega **5**, 14619 (2020).

[8] Y. Bae et al., Nano Lett. **20**, 8704 (2020).

[9] C. Wang, Q. Qiao, T. Shokuhfar, and R. F. Klie, Adv. Mater. **26**, 3410 (2014).

[10] M. Wojcik, M. Hauser, W. Li, S. Moon, and K. Xu, Nat. Commun. **6**, 7384 (2015).

[11] S. Keskin and N. de Jonge, Nano Lett. **18**, 7435 (2018).

[12] H. Wang, B. Li, Y.-J. Kim, O.-H. Kwon, and S. Granick, Proc. Natl. Acad. Sci. U. S. A. **117**, 1283 (2020).

[13] Z.-L. Xu, S. J. Kim, D. Chang, K.-Y. Park, K. S. Dae, K. P. Dao, J. M. Yuk, and K. Kang, Energy Environ. Sci. **12**, 3144 (2019).

[14] H. K. Seo, Y. Hwa, J. H. Chang, J. Y. Park, J. S. Lee, J. Park, E. J. Cairns, and J. M. Yuk, Nano Lett. **20**, 2080 (2020).

[15] D. Shin, J. B. Park, Y.-J. Kim, S. J. Kim, J. H. Kang, B. Lee, S.-P. Cho, B. H. Hong, and K. S. Novoselov, Nat. Commun. **6**, 6068 (2015).

[16] J. Yang, S. B. Alam, L. Yu, E. Chan, and H. Zheng, Micron **116**, 22 (2019).

[17] Q. Kim, D. Shin, J. Park, D. A. Weitz, and W. Jhe, Appl. Nanosci. **11**, 1 (2021).

[18] S. Hirokawa, H. Teshima, P. Solís-Fernández, H. Ago, Y. Tomo, Q.-Y. Li, and K. Takahashi, ACS Omega **5**, 11180 (2020).

[19] S. Hirokawa, H. Teshima, P. Solís-Fernández, H. Ago, Q.-Y. Li, and K. Takahashi, Langmuir **37**, 12271 (2021).

[20] Y. Sasaki, R. Kitaura, J. M. Yuk, A. Zettl, and H. Shinohara, Chem. Phys. Lett. **650**, 107 (2016).

[21] M. Textor and N. de Jonge, Nano Lett. **18**, 3313 (2018).

[22] W. Xin, I. M. De Rosa, P. Ye, L. Zheng, Y. Cao, C. Cao, L. Carlson, and J.-M. Yang, J. Phys. Chem. C **123**, 4523 (2019).

[23] P. M. G. Deursen, R. I. Koning, V. Tudor, M.-A. Moradi, J. P. Patterson, A. Kros, N. A. J. M. Sommerdijk, A. J. Koster, and G. F. Schneider, Adv. Funct. Mater. **30**, 1904468 (2020).

[24] J. Zhang et al., Adv. Mater. **29**, (2017).

[25] L. Wang et al., Angew. Chem. Int. Ed Engl. **59**, 15734 (2020).

[26] J. Lu, Z. Aabdin, N. D. Loh, D. Bhattacharya, and U. Mirsaidov, Nano Lett. **14**, 2111 (2014).

[27] T. Malis, S. C. Cheng, and R. F. Egerton, J. Electron Microsc. Tech. **8**, 193 (1988).

[28] D. J. Kelly, M. Zhou, N. Clark, M. J. Hamer, E. A. Lewis, A. M. Rakowski, S. J. Haigh, and R. V. Gorbachev, Nano Lett. **18**, 1168 (2018).

[29] S. M. Ghodsi, S. Anand, R. Shahbazian-Yassar, T. Shokuhfar, and C. M. Megaridis, ACS Nano **13**, 4677 (2019).

[30] S. M. Ghodsi, S. Sharifi-Asl, P. Rehak, P. Král, C. M. Megaridis, R. Shahbazian-Yassar, and T. Shokuhfar, Adv. Mater. Interfaces **7**, 1901727 (2020).

[31] Q.-Y. Li, K. Xia, J. Zhang, Y. Zhang, Q. Li, K. Takahashi, and X. Zhang, Nanoscale **9**, 10784 (2017).

[32] C. A. Schneider, W. S. Rasband, and K. W. Eliceiri, Nat. Methods **9**, 671 (2012).

[33] J. E. Sader, J. W. M. Chon, and P. Mulvaney, Rev. Sci. Instrum. **70**, 3967 (1999).

[34] N. M. Schneider, M. M. Norton, B. J. Mendel, J. M. Grogan, F. M. Ross, and H. H. Bau, J. Phys. Chem. C **118**, 22373 (2014).

[35] S. Keskin, C. Pawell, and N. de Jonge, Micron **149**, 103109 (2021).

[36] D. Vella, A. Ajdari, A. Vaziri, and A. Boudaoud, J. R. Soc. Interface **9**, 448 (2012).

[37] D. G. Papageorgiou, I. A. Kinloch, and R. J. Young, Prog. Mater Sci. **90**, 75 (2017).

[38] C. Lee, X. Wei, J. W. Kysar, and J. Hone, Science **321**, 385 (2008).

[39] C. S. Ruiz-Vargas, H. L. Zhuang, P. Y. Huang, A. M. van der Zande, S. Garg, P. L. McEuen, D. A. Muller, R. G. Hennig, and J. Park, Nano Lett. **11**, 2259 (2011).

[40] T. Björkman, A. Gulans, A. V. Krasheninnikov, and R. M. Nieminen, Phys. Rev. Lett. **108**, 235502 (2012).

[41] E. Khestanova, F. Guinea, L. Fumagalli, A. K. Geim, and I. V. Grigorieva, Nat. Commun. **7**, 12587 (2016).

[42] J. N. Israelachvili, *Intermolecular and Surface Forces, 3rd Edition* (Academic Press, London, 2011).

[43] J. Fang, W. G. Vandenberghe, and M. V. Fischetti, Phys. Rev. B Condens. Matter **94**, 045318 (2016).

[44] J. W. Weber, V. E. Calado, and M. C. M. van de Sanden, Appl. Phys. Lett. **97**, 091904 (2010).

[45] B. Zhuang, S. Li, S. Li, and J. Yin, Carbon N. Y. **173**, 609 (2021).

[46] L. A. Belyaeva and G. F. Schneider, Surf. Sci. Rep. **75**, 100482 (2020).